

Low Temperature Superplasticity in a Nanocomposite Iron Alloy Derived From a Metallic Glass

D.J. Branagan^{1*}, Y.L. Tang², A.V. Sergueeva³, and A.K. Mukherjee³

¹*Idaho National Engineering and Environmental Laboratory, Idaho Falls, ID, 83415*

²*Argonne National Laboratory, Argonne, IL 60439*

³*University of California, Davis, CA 95616*

ABSTRACT

The focus of this research was to utilize the self assembling phenomenon in solid state transformations in order to develop nanocomposite microstructures in 'bulk' iron based materials. Mechanical deformation studies on the nanocomposite structures at room temperature revealed that although they exhibited high yield strength (975 to 1200 MPa), they were brittle and exhibited no tensile elongation. A specialized two step annealing process was utilized which involved first holding for extended times below the crystallization onset temperature to devitrify extremely fine matrix grains followed by heating to temperatures above the crystallization onset temperature for short times. By this approach, nanocomposite microstructure could be formed consisting of α -Fe, Fe₂₃C₆ and Fe₃B type triplex matrix phases on the order of 75nm in size which were stabilized by dispersions of 2 to 10 nm α -Fe precipitates along the grain boundaries and embedded in the Fe₂₃C₆ type phase. At 750°C and at a strain rate of 10⁻³s⁻¹, this stabilized nanoscale microstructure was found to exhibit superplasticity with an ultimate tensile strength of 1800 MPa and a tensile elongation of 230%. Subsequent testing using 'jump-tests' revealed that the strain rate sensitivity factor was equal to 0.51, which consistent with the microstructural observations, revealed that the main mechanism for elevated temperature deformation was grain boundary sliding/rotational processes.

INTRODUCTION

There are many approaches utilized to refine the scale of the microstructure which result in significant differences in structure, structural scale, and microstructural stability. Liquid state processing generally does not result in the refinement of grain sizes down to the nanoscale level.¹ After nucleation has begun, growth processes are just too rapid due to the high diffusivity of atoms in the liquid state. Even at very high rapid solidification rates (10⁵ to 10⁶ K/s), the refinement of the microstructure is limited to \approx 1 μ m in size although the nature of solidification may change for instance from conventional dendrite formation to the formation of 'starburst dendrites'.^{1,2}

Other routes exist to form nanocrystalline materials by consolidating solid precursors. This could involve techniques such as applications of severe plastic deformation such as in torsional straining, multiaxial isothermal forging, die-upsetting, or equal channel angular extrusion,^{3,4} Additionally, conventional powder metallurgy could be used to consolidate heavily cold worked mechanically alloyed powder or nanopowders.⁵ Other consolidation methods exist to form nanoscale thin films or coatings via electrical deposition, pulsed electrical deposition, and thermal spraying of nanopowders.^{6,7} The

* Corresponding author now at The Nanosteel Company

problem with these aforementioned routes is that the microstructure and macrostructure is often nonuniform and contains a significant fraction of physical defects such as porosity, oxide formation, and contamination. Additionally, due to the high amount of residual stress in mechanically worked samples or prior particle boundaries resulting from micron or nanopowder consolidation, the resulting microstructures generally coarsen rapidly or even recrystallize upon the application of heat. Typically, these ripening phenomena occur at temperatures below 0.5 of the melting temperature.⁸

An alternate approach is to create uniform nanoscale structures in bulk materials in a controlled manner is to utilize the self-assembling phenomenon in solid state transformations. This type of transformation involves decomposition of single phase supersaturated solid solutions into multiphase nanoscale microstructures. During the solid state transformation, the newly formed phases self-assemble directly into characteristic nanoscale structures with an intimate mixture of phases dependent on the type of transition. The self-assembled solid state nanostructures can be prepared using a number of distinct metallurgical approaches such as spinodal decompositions, eutectoid transformations, or glass devitrification in a wide variety of metallic systems.^{8,9} The approaches share the common feature that they start with samples of uniform composition on both a macroscopic and microscopic scale.

In this paper, the approach utilized is to quench a specially modified iron based system in a metallic glass state and then devitrify the glass state into a multiphase nanostructured sample. In iron based systems, depending on the specific composition, the crystallization temperatures generally varies from 500°C to 650°C and the enthalpy of the glass to crystalline transformation varies from -75 J/g to -200 J/g.¹⁰ Since the melting temperature is often reduced to 1100 to 1200°C, this means that the glass devitrification occurs at low fractions of the melting temperature ($\approx 0.5T_m$) where the driving force for crystallization, due to the metastable nature of the glass state, is extremely high, but grain growth is still sluggish. This results in a very high nucleation frequency with limited time for grain growth before impingement between neighboring grains occurs. Thus, the solid/solid state glass devitrification can be represented as an enabling transformation towards the development of nanoscale microstructures in bulk materials. Additionally, these devitrified microstructures are generally stable to at least 0.7 to 0.8 of the melting temperature.^{8,11} An additional advantage of this route, is that macrodefects such as porosity or cracks, inherent to many other approaches, can be virtually eliminated.

When the microstructure is reduced to the nanoscale level, a high percentage of the atoms in the material ($\approx 30\%$) are associated with the grain boundaries and an extremely high density of 2-d defect interfaces such as phase and grain boundaries reside in the microstructure. The 2-d defect boundaries can interact in a complex manner with dynamic processes occurring during deformation. Superplasticity is one well established phenomenon which is found to be very dependant on microstructural scale and can be described by the constitutive Mukherjee-Bird-Dorn (MBD) relation.^{12,13} This relation shows that the achievement of nanoscale grain sizes could lead to increases in plasticity, reductions in the superplastic temperature range, and increases

in the superplastic strain rates. In this paper, we will explore this phenomena in a nanocrystalline iron based alloy formed via devitrification from a metallic glass precursor

EXPERIMENTAL PROCEDURE

The alloy composition designed for the studies described in this paper had the following atomic stoichiometry; $(\text{Fe}_{0.8}\text{Cr}_{0.2})_{79}\text{B}_{17}\text{W}_2\text{C}_2$. The targeted alloy was processed from high purity constituents (>99.9%) into two ribbons by melt-spinning in 1/3 atm He at a wheel tangential velocity of 15 m/s. Heat-treating was done on the ribbon and ingot samples in a radiating vacuum furnace at 10^{-6} torr. The samples were heated from room temperature at a 120°C/min heating rate to the heat treatment temperature, held for a constant 1 hour annealing time, and then furnace cooled. Differential thermal analysis (DTA) and Differential Thermal Calorimetry (DSC) of the ribbon samples was performed in a Perkin Elmer DTA-7 from 30°C to 1375°C at a heating rate of 10°C/min in a 50 ml/s flowrate of UHP Ar. X-ray diffraction was carried out on powdered samples after incorporation of a silicon standard using a Bruker X-ray Diffractometer with Cr-K_α radiation. Analysis of the experimental X-ray patterns was done by Rietveld analysis using SIROQUANT V 2.0 software and the calculated patterns were refined until the total χ^2 was less than 3.5 over the entire two-theta range (40°-150°). Transmission Electron microscopy (TEM) was performed on a Philips CM30T analytical electron microscope attached with an EDAX energy dispersive spectrometer (EDS) using an ultra thin window detector. TEM samples were first polished from the free side of the ribbons to reduce the thickness to $\approx 20 \mu\text{m}$, dimpled and then ion milled by a Gatan PIPS low angle ion miller from two directions. For composition analysis using EDS, a separate spectrum was collected for the beam directed through the hole of each thin specimen and then this 'hole count' was subtracted from the unknown and standard spectra to minimize effects of spurious X-ray generation within the AEM. Peak intensities were converted to compositions using the Cliff–Lorimer approach, $I_A/I_B = k_{AB} * C_A/C_B$ where B is the base element (iron in this case) for which the k-factors are determined.¹⁴ Convergent beam electron diffraction (CBED) was employed to analyze the structure and identify the nano-sized phases. Tensile tests were done on a custom-built computer controlled constant strain rate tensile test machine with a displacement resolution of 5 μm and a load resolution of 0.1 N.

RESULTS and DISCUSSION

As-Solidified Structure

The as-solidified structure of the melt-spun ribbons was studied using both X-ray diffraction and DTA/DSC thermal analysis. The as-spun X-ray diffraction pattern is shown in the bottom graph of Figure 1. The lack of Bragg diffraction peaks (not including the silicon standard), indicates that the as-solidified structure is amorphous. The DTA scan with the glass to crystalline transformation and melting peaks labeled in the as-spun alloy is shown in Figure 2. At the onset temperature of 536°C, the glass was found to exhibit a high enthalpy of crystallization (−119 J/g) and crystallized at a very rapid transformation rate (0.019/s). The magnitude of the enthalpy in combination with the X-ray scan indicates that the as-solidified structure is nominally 100% amorphous.

Devitrified Structure

The glass samples were heat treated at 850°C for one hour in order to cause complete devitrification along with limited grain growth to coarsen the nanoscale structure. By this approach, the phases could be more easily identified using microdiffraction in conjunction with EDS in the TEM. Microstructure analysis revealed that the devitrified microstructure contained three phases which are approximately the same size (250 nm) and are separated by 'clean' grain boundaries with the absence of distinct or continuous grain boundary precipitates. Once the CBED patterns were analyzed and the phases were identified, the individual phases could be easily distinguishable due to their distinct appearance/morphology (Figure 3). The microstructure consists of three phases (α -Fe, Fe_{23}C_6 and Fe_3B) of almost identical sizes. The α -Fe phase forms a distinctly mottled structure, the Fe_{23}C_6 type phase forms a featureless smooth structure, and the Fe_3B phase forms a heavily multi-twinned structure. Note that the Fe_{23}C_6 and Fe_3B phases are not known to form in their respective binary systems but can form as stable phases due to the presence of impurities or solute atoms.^{15,16} Additionally, the EDS scans taken on the individual phases revealed that each phase also contained dissolved Cr, W, B, and C atoms. The experimental and calculated X-ray diffraction patterns of the 850°C sample are shown in Figure 4. In agreement with the CBED results, the same three phases were found; cubic α -Fe with an $\text{Im}3\text{m}$ space and $a = 2.873 \text{ \AA}$, cubic Fe_{23}C_6 with an $\text{Fm}3\text{m}$ space group and $a = 10.639 \text{ \AA}$, and tetragonal Fe_3B with an I-4 space group and $a = 8.630 \text{ \AA}$ and $c = 4.288 \text{ \AA}$. Note that all of the phases had significantly different lattice parameters compared to their respective unalloyed binary phases indicating significant amounts of dissolved solute atoms in agreement with the EDS results.

Low Temperature Crystallization

From low temperature relaxation, recovery, and crystallization studies, it was found that the devitrified microstructure could be changed significantly leading to large changes in properties.¹⁷ To study this effect, samples of the ribbon were heat treated below the crystallization onset temperature (536°C) and were annealed at 500°C and for 100 hours. The X-ray diffraction scan illustrating the structural changes that occurred during this low temperature heat treatment is shown in the top curve of Figure 1. It can be seen that during the 500°C heat treatment, α -Fe ($a = 2.864 \text{ \AA}$) and Fe_3B ($a = 8.613$ and $c = 4.322$) phases crystallized. The TEM micrograph of this 500°C heat treated sample can be seen in Figure 5a. It was found that an extremely fine microstructure formed consisting of a Fe_3B matrix grains typically from 20-50 nm in size with second phase nanoscale α -Fe precipitates forming both along the subgrain boundaries and embedded within the matrix of Fe_3B phase. Also, from the micrograph, it is clear that there are regions where crystallization is not complete.

To initiate complete crystallization, the 500°C heat treated ribbons were additionally annealed at 700°C for 10 minutes. TEM studies show that after the 700°C heat treatment, the microstructure is three phase consisting of α -Fe, Fe_{23}C_6 , and Fe_3B (Figure 5b). Thus, during the 700°C heat treatment, the Fe_{23}C_6 phase formed. Note that with respect to phase content, phase distribution, and grain boundary character, the

microstructure is similar to that obtained after one step annealing at 850°C for 1 hour (see Figure 3). However, the scale of the phases is much finer (~75 nm) compared to the higher temperature anneal (~250 nm). Additionally, a very fine distribution of 2-10 nm α -Fe precipitates is found along some of the grain boundaries and also embedded in the Fe_{23}C_6 phase. It is thought that the presence of these iron nano-precipitates will provide additional Zener pinning to stabilize the microstructure against grain growth at elevated temperature.

Mechanical Deformation Studies

A series of tests were done to explore the tensile properties of the devitrified microstructure. Long uniform segments of ribbon were annealed for one hour at 600°C, 650°C, and 750°C and were tensile tested at 20°C at a strain rate of 10^{-3}s^{-1} . It was found that the alloys were completely brittle with no tensile elongation and ultimate strengths from 975 to 1200 MPa (Figure 6).

Due to the nanoscale grain size of the devitrified structure, studies were then launched at elevated temperature to see if the material exhibited low temperature superplasticity. Based on the studies shown earlier on stabilizing the microstructure, before mechanical testing, the ribbon segments were heat treated at 500°C for 100 hours to initiate a high nucleation frequency while limiting growth and then annealed at 600°C for one hour to cause complete devitrification while minimizing subsequent grain growth. The tensile properties were then tested in a region where superplasticity may exist specifically at 750°C ($0.7 T_m$) and at a strain rate of 10^{-3}s^{-1} . This sample was found to exhibit a very high tensile elongation of 230% with an ultimate strength of 1800 MPa (Figure 7). Achieving this magnitude of strength at such a high homologous temperature of 0.7 is very significant.

The high elongation measured at 750°C is indicative of low temperature superplasticity but does not a priori identify the mechanism as superplasticity. Superplasticity involves an inherent resistance to strain localization by necking in tension tests. It also requires maintaining grain continuity during three-dimensional grain boundary sliding via various accommodation processes including grain boundary migration, grain rotation, diffusion, and dislocation motion. Thus, to shed some light on deformation mechanisms, a 'jump-test' was done at 750°C using various strain rates on a stabilized nanocomposite sample heat treated as before (Figure 8). By plotting out the stress versus the strain rate, the strain rate sensitivity factor was determined to be 0.51 (Figure 9). This value is indeed indicative of the operation of superplasticity by a grain boundary sliding mechanism. Further investigation is underway in order to identify the other rate parameters for the manifestation of superplasticity.

Microstructural Analysis of Superplastic Sample

The fracture surface of the sample superplastically deformed during the jump test was analyzed in the SEM (Figure 10). The fracture surface exhibits an equiaxed structure consisting of generally spherical submicron dimples, which are normal to the elongation direction. The appearance of the fracture surface is consistent with a microvoid coalescence mechanism of failure arising from plastic flow. The presence of the

microvoids indicates that the utilized strain rate of the last step of the 'jump-test' may have been too fast to allow for diffusional relaxation processes to completely avoid microvoid nucleation.

A TEM sample was made from the fracture surface and the microstructure was observed at a distance of 0.5 mm off the fracture edge. Analysis of the microstructure showed it was three phase consisting of α -Fe, Fe_{23}C_6 , and Fe_3B phases consistent with the results from elevated temperature annealing studies (Figure 11). A general texture was discovered with a $\langle 020 \rangle$ orientation of the Fe_{23}C_6 phase in the deformation direction, which can be seen in Figure 12. Additionally, evidence existed for dislocation glide inside the Fe_{23}C_6 and α -Fe phases. Because the observed final strain rate was too high, some grains were elongated and there was also some dislocation slip, however the main mechanism appears to be grain boundary sliding/rotation. Additionally, some intergranular cracks were observed parallel to the deformation direction and along the grain boundaries of the Fe_{23}C_6 phase. No cracking was observed in the α -Fe and Fe_3B phases. More detailed analysis and subsequent studies will be needed to clarify the complex deformation mechanism in this nanoscale multiphase material.

CONCLUSIONS

In this paper, a novel approach was utilized to develop nanocomposite microstructures in bulk iron based materials by utilizing the self assembling phenomenon in solid state transformations. This approach results in both full density and temperature stabilized nanocomposite microstructures which are generally not possible to achieve via other routes/approaches used to develop nanoscale structures in bulk materials. Furthermore, through careful manipulation of the devitrification pathway and utilizing recovery, relaxation, and crystallization phenomena, it was found that significant refinement occurred in the size and distribution of the matrix phases and second phase precipitates. Through a specialized two stage heat treatment, a nanocomposite microstructure could be formed consisting of α -Fe, Fe_{23}C_6 , and Fe_3B type triplex matrix phases on the order of 75 nm in size which were stabilized by dispersions of 2 to 10 nm α -Fe precipitates along the grain boundaries and embedded in the Fe_{23}C_6 type phase. This stabilized microstructure was found to exhibit at 750°C, a tensile elongation of 230% and an ultimate tensile strength of 1800 MPa. Subsequent testing using 'jump-tests' revealed that the strain rate sensitivity factor was equal to 0.51, which consistent with the microstructural observations, revealed that the main mechanism for elevated temperature deformation was grain boundary sliding/rotational processes. Thus, this paper shows the first reported evidence of superplasticity from a material derived from an amorphous precursor and acts as a beacon toward the usage of materials derived from amorphous materials in structural applications.

ACKNOWLEDGMENT

Research was supported through the Defense Advanced Research Projects Agency (DARPA) under the DOE Idaho Operations Office Contract No. DE-AC07-99ID13727. TEM studies were performed at the Electron Microscopy Center at Argonne National Laboratory, which is operated by the University of Chicago under Contract No. W-31-

109-ENG-38. A.V. Sergueeva and A.K. Mukherjee would like to acknowledge a grant from NSF-DMR program.

REFERENCES

- [1] J.H. Perepezko and G. Wilde, *Journal of Non-Crystalline Solids* 274, 271 (2000).
- [2] D.J. Branagan, T.A. Hyde, C.H. Sellers, and R.W. McCallum, "Developing Rare Earth Permanent Magnet Alloys For Gas Atomization", *J. Phys. D: Appl. Phys.*, 29(1996), 2376.
- [3] R.Z. Valiev, R.K. Islamgaliev, and I.V. Alexandrov, *Prog. Mater. Sci.* 45, 103 (2000).
- [4] G.A. Salishchev, O.R. Valiakhmetov, V.A. Valitov, and S.K. Mukhtarov, *Mater. Sci. Forum* Vols.170-172 (1994) p.121.
- [5] J.R.Groza, in: *Nanostructured Materials: Processing, Properties and Potential Applications*, Ed. C.C.Koch, William Andrew Publishing, Norwich, NY, 2002, p.115.
- [6] J.H. Perepezko, in: R.D. Shull, J. Joshi (Eds.), *Thermal Analysis in Metallurgy*, TMS, Warrendale, PA, 1992, p.121.
- [7] B.A. Mueller, J.H. Perepezko, *Metall. Trans. A*18(1987), 1143.
- [8] K.Lu, *Materials Science and Engineering*, R16(1996), 161.
- [9] Clavaguera-Mora M.T., Clavaguera N., Crespo D., Pradell T. *Prog. Mater.Sci.* 47(2002), 559.
- [10] D.J. Branagan, The Nanosteel Company, unpublished research.
- [11] D.J. Branagan, M.J. Kramer, and R.W. McCallum, "Transition Metal Carbide Formation in the Nd₂Fe₁₄B System and Potential as Alloying Additions", *J. Alloys. and Compounds*, 244(1996), 27-39.
- [12] A. K. Mukherjee, J. E. Bird and J. E. Dorn, *Trans. ASM.*, 62 (1969) 155.
- [13] A.K.Mukherjee, *Mater. Sci. Eng.* A323 (2002) 318.
- [14] G. Cliff, F.W. Lorimer, *J. Microscopy* 103 (1975) 203.
- [15] R. Coehoorn R, D.B. De Mooij, and C. De Waard, "Melt-Spun Permanent Magnet Materials Containing Fe₃B as the Main Phase", *J. Magn. Magn. Mater.*, 80(1989), 101-104.
- [16] RWK Honeycombe and HKDH Bhadeshia, STEELS Microstructure and Properties, Halsted Press, New York, 2nd ed., 1995, p192.
- [17] B.B. Kappes, B.E. Meacham, Y. Tang, and D.J. Branagan, "Relaxation, Recovery, Crystallization, and Recrystallization Transformations in Iron Based Amorphous Precursors", submitted, Nanotechnology.

Figures:

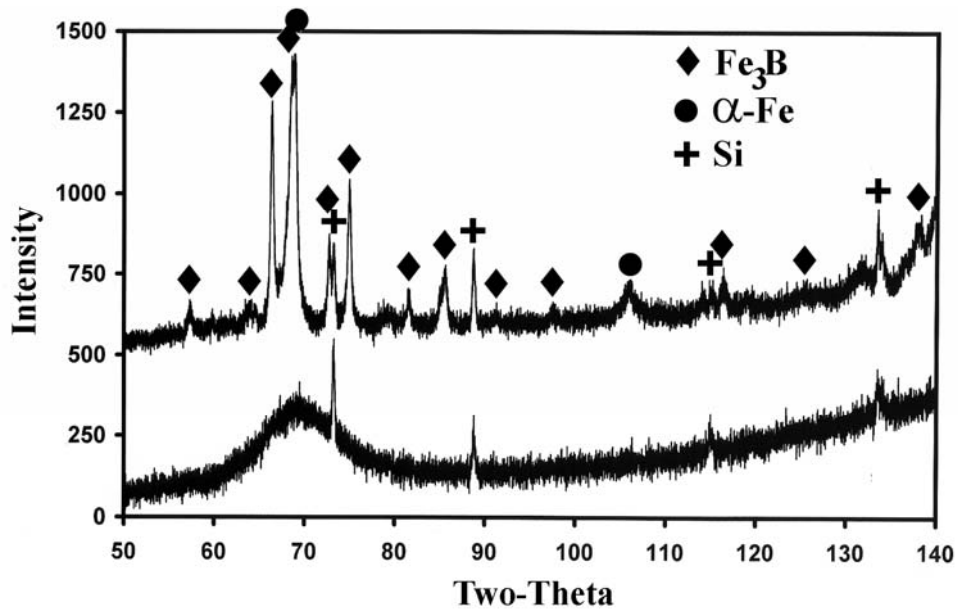


Figure 1 X-ray diffraction diagrams for the as-solidified (bottom curve) and 500°C for 100 hours heat treated (top curve) ribbons. Note that a silicon standard was incorporated for lattice parameter determination.

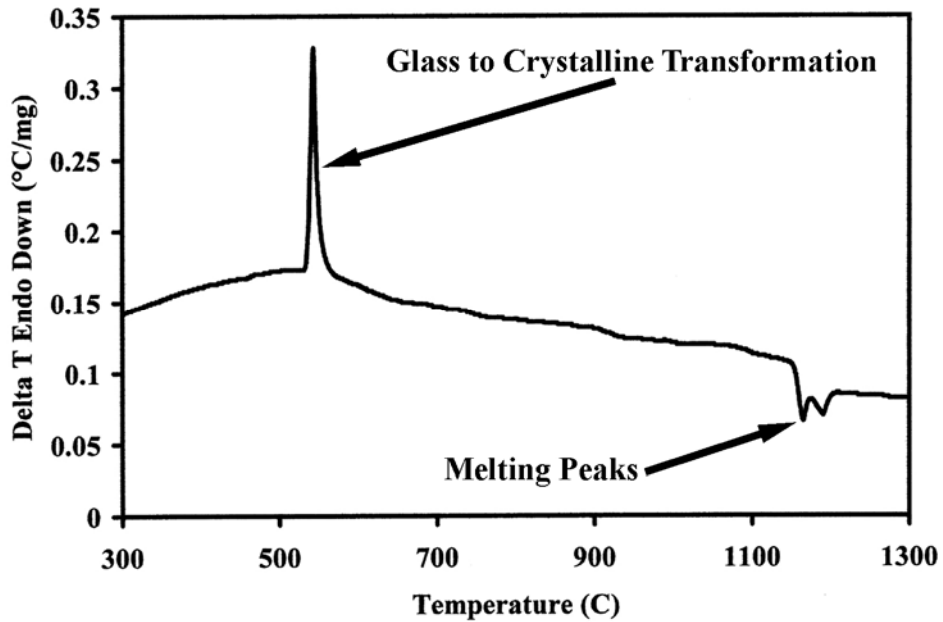


Figure 2 DTA scan of the as-spun melt-spun ribbon. The extremely sharp glass to crystalline peak and melting peaks are identified on the diagram.

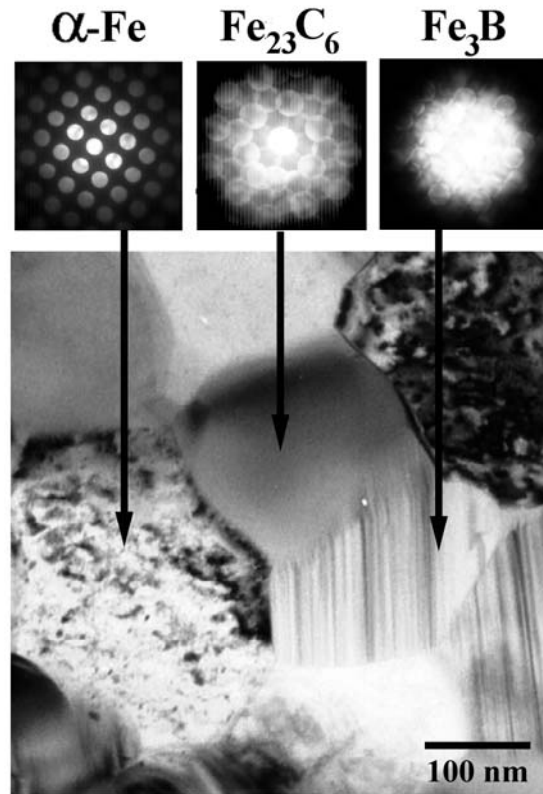


Figure 3 TEM micrograph showing the microstructure after annealing for 850°C for 1 hour. The coarsened phases could be easily identified using convergent beam electron diffraction as shown in the by insets above.

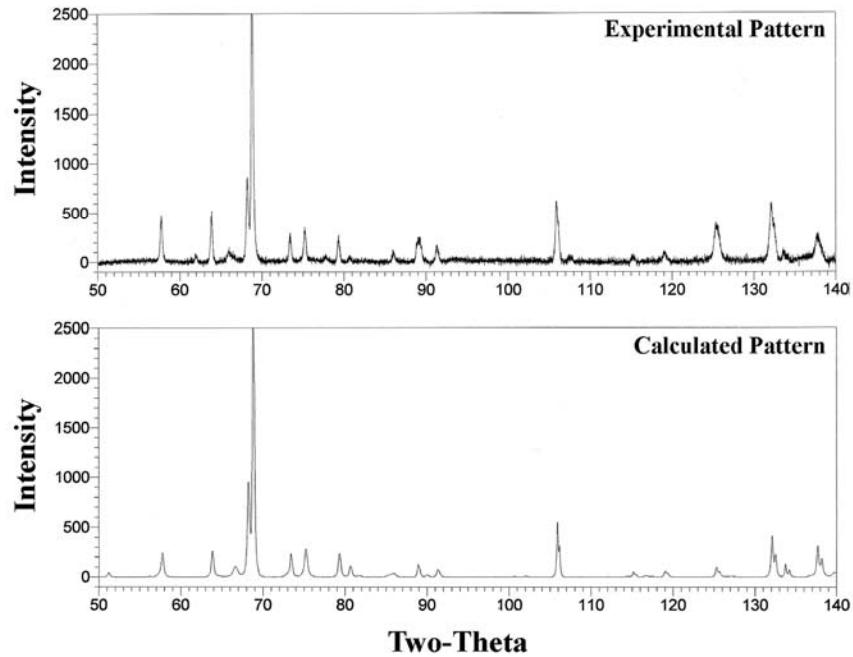


Figure 4 Experimental and Rietveld calculated patterns for the ribbon sample heat treated at 850°C for 1 hour. Note that silicon was added to the powdered sample as a standard to adjust for instrumental two-theta errors.

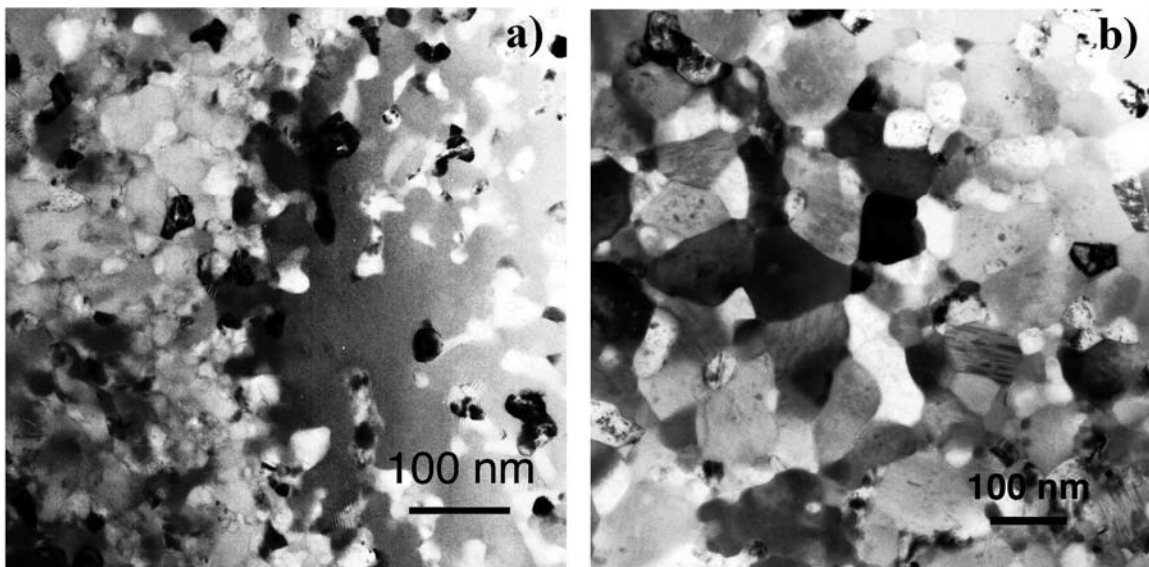


Figure 5 TEM micrographs showing microstructure of: a) 500°C for 100 hour sample and b) 500°C for 100 hour -700°C for 10 minute sample.

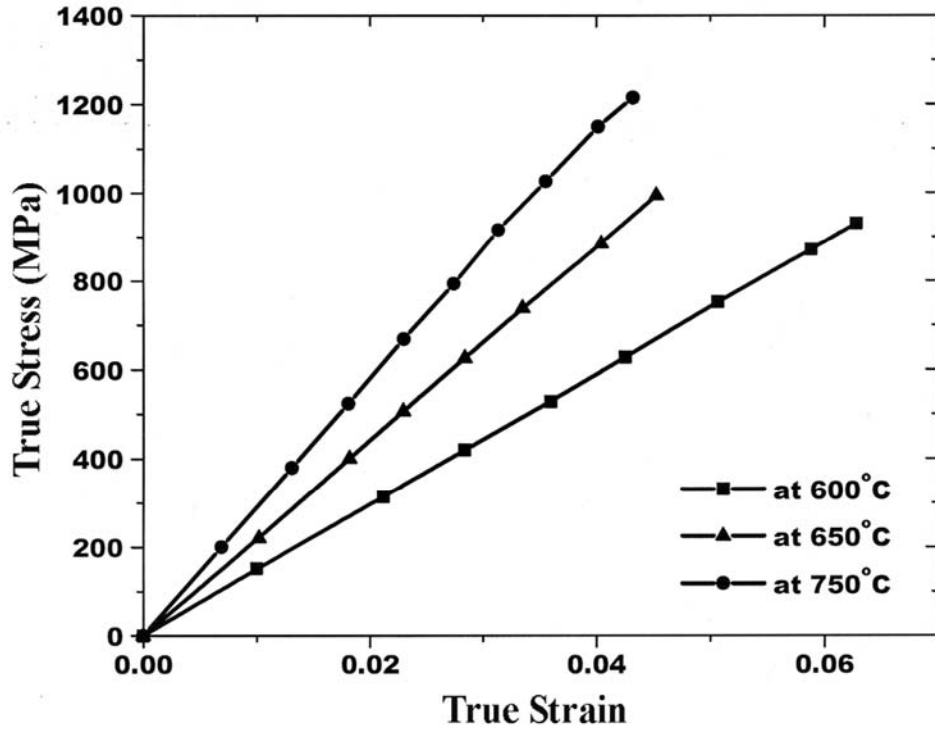


Figure 6 Tensile studies at room temperature on samples heat treated at 600°C, 650°C, and 750°C.

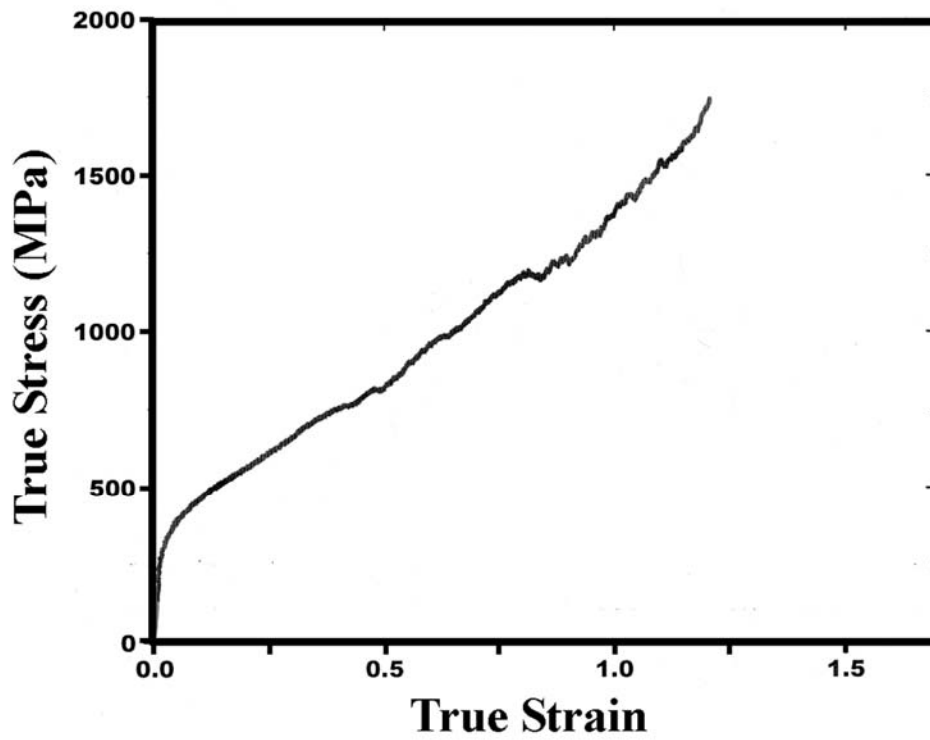


Figure 7 Tensile studies at 750°C on samples heat treated at 500°C for 100 hours and 600°C for 1 hour.

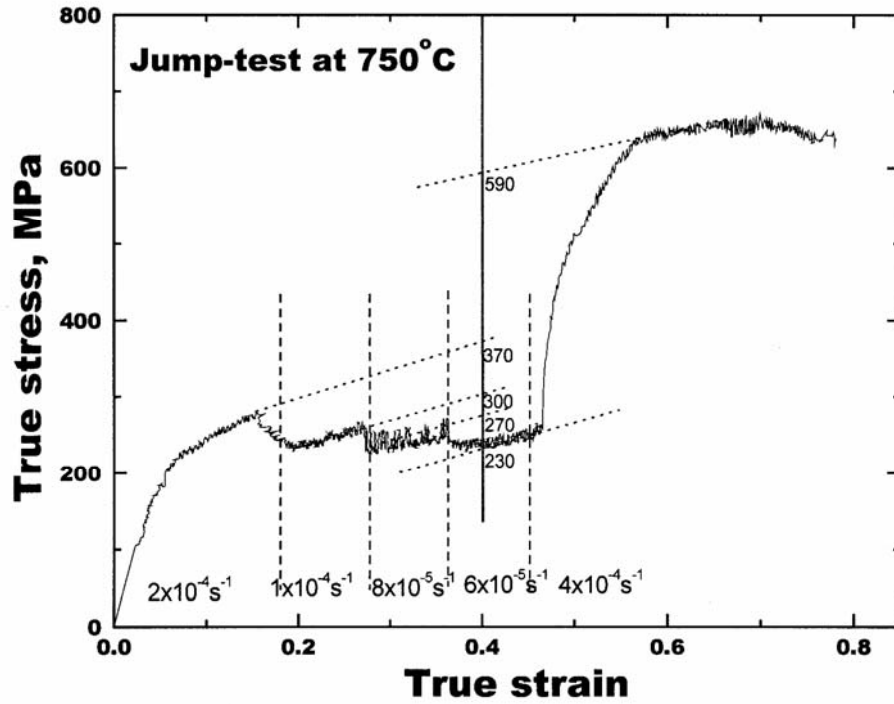


Figure 8 Jump test at 750°C on sample heat treated at 500°C for 100 hours.

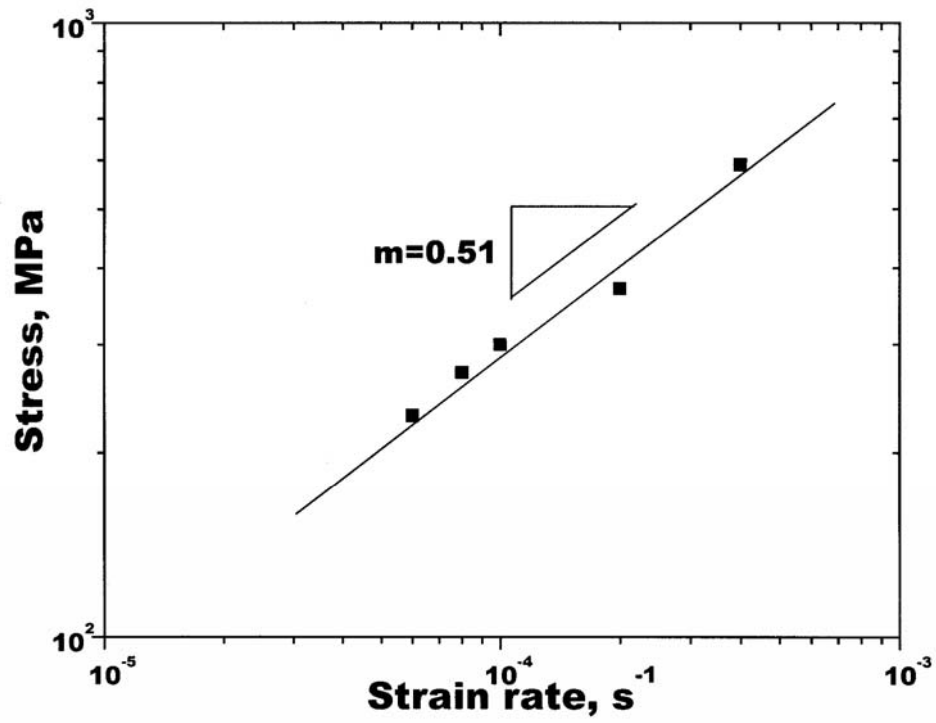


Figure 9 Log stress versus log strain rate data showing the strain rate sensitivity exponent.

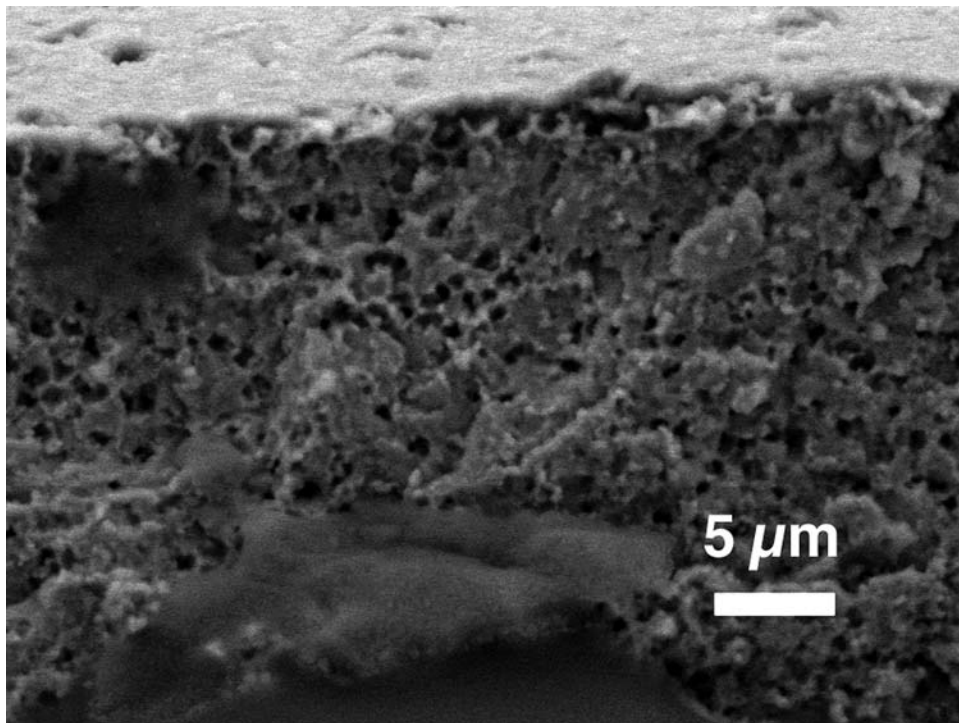


Figure 10 SEM micrograph of the cross section of the fracture surface of the sample used for the 'jump-test'.

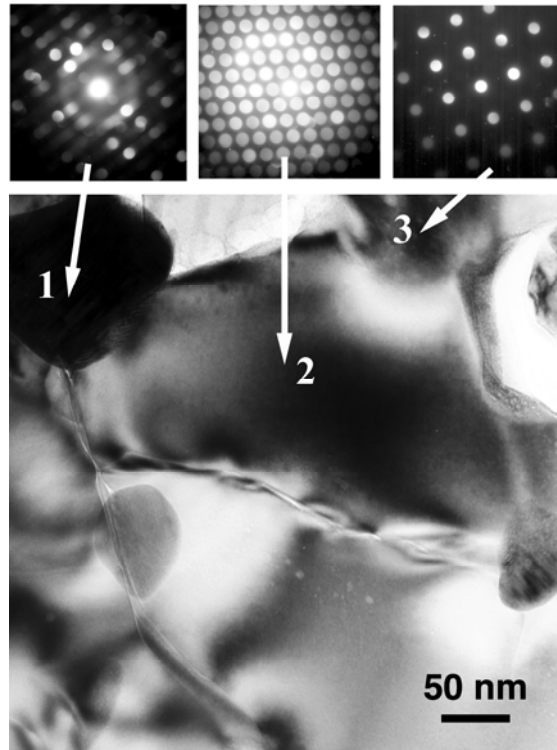


Figure 11 TEM micrograph of the sample exhibiting superplasticity showing the identification of the phases: phase 1- Fe_3B , phase 2- Fe_{23}C_6 and phase 3 - α -Fe.

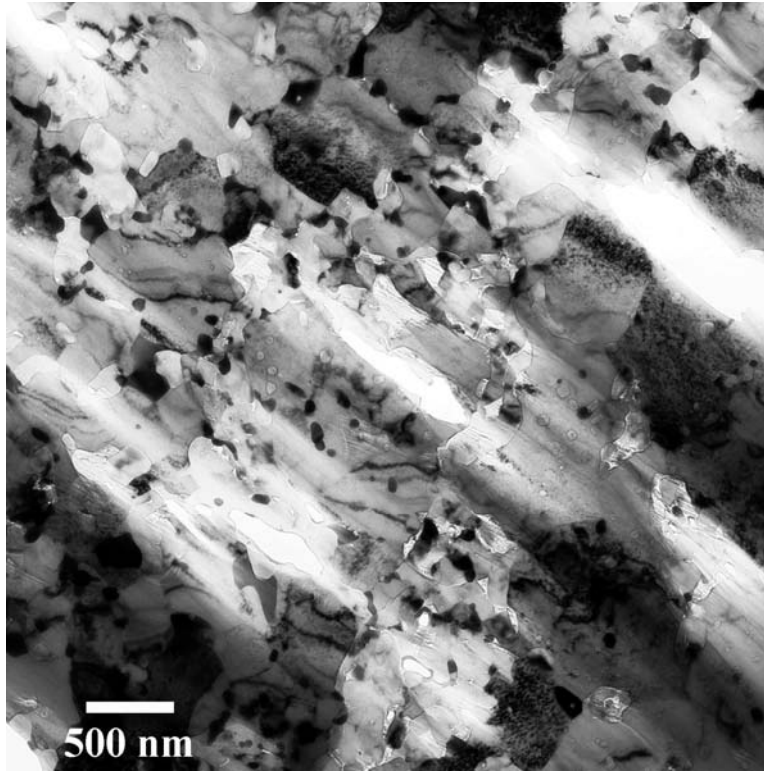


Figure 12 TEM micrograph of superplastically deformed region showing the elongated grains and the general $\langle 020 \rangle$ texture.